J|A|C|S
ARTICLES
Published on Web 02/02/2002

Sandia Octahedral Molecular Sieves (SOMS): Structural and Property Effects of Charge-Balancing the M^{IV}-Substituted (M = Ti, Zr) Niobate Framework

May Nyman,[†] Akhilesh Tripathi,[‡] John B. Parise,[‡] Robert S. Maxwell,[§] and Tina M. Nenoff*[,†,⊥]

Sandia National Laboratories, MS-0755, P.O. Box 5800, Albuquerque, New Mexico 87185, Department of Chemistry and Department of Geosciences, State University of New York, Stony Brook, New York 11794-2100, and Lawrence Livermore National Laboratory, P.O. Box 808, L-226, Livermore, California 94551

Received September 14, 2001

Abstract: Sandia octahedral molecular sieves (SOMS) is an isostructural, variable composition class of ion exchangers with the general formula $Na_2Nb_{2-x}M^{IV}_xO_{6-x}(OH)_x \cdot H_2O$ (M^{IV} = Ti, Zr; $x = 0.04-0.40$) where up to 20% of the framework Nb^V can be substituted with Ti^{IV} or Zr^{IV}. This class of molecular sieves is easily converted to perovskite through low-temperature heat treatment (500−600 °C). This report provides a detailed account of how the charge imbalance of this Nb^V-M^{IV} substitution is compensated. X-ray powder diffraction with Rietveld refinement, infrared spectroscopy, thermogravimetric analysis, ^{23}Na MAS NMR, and ^{1}H MAS NMR were used to determine how the framework anionic charge is cation-balanced over a range of framework compositions. All spectroscopic evidence indicated a proton addition for each M^{IV} substitution. Evidences for variable proton content included (1) increasing OH observed by ^{1}H MAS NMR with increasing M^{IV} substitution, (2) increased infrared band broadening indicating increased H-bonding with increasing M^{IV} substitution, (3) increased TGA weight loss (due to increased OH content) with increasing M^{IV} substitution, (4) no variance in population on the sodium sites (indicated by Rietveld refinement) with variable composition, and (5) no change in the ^{23}Na MAS NMR spectra with variable composition. Also observed by infrared spectroscopy and ^{23}Na MAS NMR was increased disorder on the Nb^V/M^{IV} framework sites with increasing M^{IV} substitution, evidenced by broadening of these spectral features. These spectroscopic studies, along with ion exchange experiments, also revealed the effect of the Nb^V/M^{IV} framework substitution on materials properties. Namely, the temperature of conversion to $NaNb_{1-x}M^{IV}_xO_3$ (M = Ti, Zr) perovskite increased with increasing Ti in the framework and decreased with increasing Zr in the framework. This suggested that Ti stabilizes the SOMS framework and Zr destabilizes the SOMS framework. Finally, comparing ion exchange properties of a SOMS material with minimal (2%) Ti to a SOMS material with maximum (20%) Ti revealed the divalent cation selectivity of these materials which was reported previously is a function of the M^{IV} substitution in the framework. A thorough investigation of this class of SOMS materials has revealed the importance of understanding the influence of heterovalent substitutions in microporous frameworks on material properties.

Introduction

Framework metal substitutions in microporous materials that enhance catalytic activity,[1−7] ion exchange behavior,[8−12] and stability[13] have been discovered both by accident and by design. The heteroatomic substitutions alter material functionality by way of charge, size, electronegativity, and binding behavior that differ from the bulk framework metals. Through substitution of Ti or Zr in a nominal $NaNbO_3$ octahedral framework, we have produced a new family of isostructural $Na_2Nb_{2-x}M^{IV}_xO_{6-x}(OH)_x \cdot H_2O$ (M^{IV} = Ti, Zr; $x = 0.03-0.40$) microporous materials, know as SOMS (Sandia octahedral molecular sieves).[14] In an initial Communication,[15] we

[†] Sandia National Laboratories.
[‡] State University of New York.
[§] Lawrence Livermore National Laboratory.
[⊥] E-mail: tmnenof@sandia.gov.

(1) Prakash, A. M.; SungSuh, H. M.; Kevan, L. *J. Phys. Chem. B* **1998**, *102*, 857.
(2) Yang, S. M.; Lin, J. Y.; Guo, D. H.; Liaw, S. G. *Appl. Catal.* **1999**, *181*, 113.
(3) Notari, B. *Adv. Catal.* **1996**, *41*, 253.
(4) Castro-Martins, S. d.; Khouzami, S.; Tuel, A.; Taarit, Y. B.; Murr, N. E.; Sellami, A. *J. Electranal. Chem.* **1993**, *350*, 15.
(5) Bhaumik, A.; Inagaki, S. *J. Am. Chem. Soc.* **2001**, *123*, 691.
(6) Zhang, J. L.; Matsuoka, M.; Yamashita, H.; Anpo, M. *J. Synchrotron Radiat.* **2001**, *8*, 637.
(7) Krijnen, S.; Sanchez, P.; Jakobs, B. T. F.; vanHooff, J. H. C. *Microporous Mesoporous Mater.* **1999**, *31*, 163.
(8) Dedecek, J.; Cejka, J.; Wichterlova, B. *Appl. Catal. B* **1998**, *15*, 233.
(9) Eapen, M. J.; Reddy, K. S. N.; Joshi, P. N.; Shiralkar, V. P. *J. Inclusion Phenom. Mol. Recognition Chem.* **1992**, *14*, 119.
(10) Singh, A. P.; Reddy, K. R. *Zeolites* **1994**, *14*, 290.
(11) Behrens, E. A.; Poojary, D. M.; Clearfield, A. *Chem. Mater.* **1998**, *10*, 959.
(12) Ouki, S. K.; Kavannagh, M. *Water Sci. Technol.* **1999**, *39*, 115.
(13) Shen, S. C.; Kawi, S. *J. Phys. Chem. B* **1999**, *103*, 8870.
(14) Nenoff, T. M.; Nyman, M. A New Class of Inorganic Molecular Sieves: Sodium Niobium Metal Oxides. U.S. Patent, submitted, 2001.

10.1021/ja017081z CCC: $22.00

reported the structure of one member of this family, SOMS-1 ($Na_2Nb_{1.6}Ti_{0.4}O_{5.6}(OH)_{0.4}\cdot H_2O$), based on data collected at the Brookhaven National Laboratory National Synchrotron Light Source (BNL, NSLS) on a $5 \times 8 \times 8$ μm nonmerohedrally twinned crystal. Additionally, we introduced the unique properties of SOMS such as its one-step thermal decomposition to perovskite and high affinity for sorption of divalent metals over univalent metals. In this follow-up study, we report in-depth characterization of SOMS as a variable-composition class of materials, with a particular focus on the effect of varying the M^{IV} concentration on the synthesis, composition, structure, stability, and ion exchange properties of SOMS.

Numerous examples of metal-substituted, tetrahedral framework, microporous materials can be found in the recent literature. Of particular pertinence to this report are materials whose ion exchange properties are influenced by framework substitutions. For instance, substitution of Al^{III} or Ga^{III} for Si^{IV} in silicate-based zeolites greatly enhances ion exchange capacity by increasing the negative charge on the framework and thus increasing the number of exchangeable cations.[9,10,12] Similarly, substitution of Mg^{II} or Zn^{II} for Al^{III} on the aluminum site of an aluminophosphate framework results in increased ion exchange capacity.[8] Isoelectronic substitutions of metals with different cationic radii or electronegativities than those of the framework metals also affect ion exchange behavior of microporous, tetrahedral framework materials. For instance, replacement of Ge^{IV} for Si^{IV} in aluminosilicate (aluminogermanate) structures results in frameworks with higher $Al:M^{IV}$ ratios, which in turn increases the ion exchange capacity.[16−18] Substitution of Ge^{IV} for Si^{IV} in a titanosilicate pharmacosiderite analogue results in a phase with enhanced Cs and Sr selectivity.[11]

Analogous metal substitutions in octahedral microporous frameworks have not been investigated so extensively, primarily because in comparison to tetrahedral framework molecular sieves, there are relatively few octahedral[19−21] and mixed tetrahedral-octahedral[22] molecular sieve materials. In the titanosilicate pharmacosiderite example described above, Ge^{IV} also substitutes on the octahedral Ti^{IV} site in the selectivity-enhanced ion exchange materials.[11] Substitution of Nb^{V} on the Ti^{IV} octahedral site of crystalline silicotitanate (CST) results in greatly enhanced selectivity of Cs from solutions containing >5 molar Na.[23] In another example of metal substitution in an octahedral framework, the substitution of Cu for framework Mn in a microporous manganate resulted in increased oxidation dehydration activity and also enhanced framework stability.[2]

The discovery of the SOMS materials was unique and challenging in that the nominal "unsubstituted" $NaNbO_3$ structure had not been previously reported, nor was it readily synthesized, whereas in the above-mentioned examples of metal substitutions in microporous frameworks, the nominal composition and framework was previously known. While SOMS-1 with maximum substitution of M^{IV} (20% of Nb^{V} substituted with Ti^{IV}) was readily obtained, SOMS with greatly decreased M^{IV} concentration (<5%) proved to be unstable and was therefore more difficult to obtain in a pure form.

The study reported herein is a thorough investigation of the $Na_2Nb_{2-x}M^{IV}_xO_{6-x}(OH)_x\cdot H_2O$ (M^{IV} = Ti, Zr; $x = 0.04-0.40$) SOMS materials. Synthetic strategies which were developed to obtain the metastable SOMS of the $x < 0.4$ compositions are discussed. Framework charge and structure compensation of the SOMS M^{IV}/Nb^{V} substitution were investigated by Rietveld refinement, ^1H and ^{23}Na MAS NMR, thermogravimetry, bulk chemical analysis, and vibrational spectroscopies. The stability of the SOMS phases as a function of framework composition is investigated through thermal analysis. Finally, preliminary investigations of the ion exchange behavior as a function of framework composition are described, particularly with regard to understanding how framework composition of microporous ion exchangers may be tailored for optimum ion exchange behavior.

Experimental Section

Synthesis. Chemical Reagents. Niobium(V) ethoxide, $Nb(OC_2H_5)_5$ (99.5% purity, catalog no. 33920-2), tetraisopropyl titanium, $Ti(OC_3H_7)_4$ (99.999% purity, catalog no. 37,799-6), and zirconium isopropoxide, $Zr(OC_3H_7)_4\cdot HOC_3H_7$, were purchased from Aldrich Chemical Co. and stored and handled as received in an inert atmosphere, argon-filled box. Reagent grade sodium hydroxide pellets and a 30 wt % solution of hydrogen peroxide were purchased from Fisher, and a 70 wt % solution aqueous solution of *tert*-butyl hydroperoxide and 2,4-pentadione was purchased from Aldrich. All reagents were used as received. All reactions were carried out in solutions of deionized water.

In a typical reaction, pentaethoxyl niobium (NbOEt) and tetraisopropyl titanium (TIPT) or tetraisopropyl zirconium (ZIPT) are combined in a 4:1−50:1 $Nb:M^{IV}$ ratio in a 20 mL glass vial in an inert atmosphere box; total NbOEt plus M^{IV} alkoxide is 2.8 mmol (for instance, for a 4:1 Nb:Ti reaction, 0.16 g (0.56 mmol) of TIPT and 0.71 g (2.24 mmol) of NbOEt are used). The vial containing the mixture of alkoxides is capped and removed from the drybox and treated ultrasonically for 10 minutes to mix thoroughly. Sodium hydroxide (1.34 g, 33.6 mmol) is dissolved in 8 mL of deionized water in a 23 mL Teflon liner for a pressurized Parr reactor vessel. While stirring, the alkoxides are added to the NaOH solution and stirred for 30 min more. The final ratio of reagents is 12:1:159; $Na:(Nb + M^{IV}):H_2O$. The final pH of the solution is around 13.7. In some cases, a "ligand" (L) is added to aid in solubilizing M^{IV}. These include 2,4-pentadione, *tert*-butylhydroperoxide, and hydrogen peroxide. The ligands are added in a 1:1 ratio of $L:(Nb + M^{IV})$, so in the ligand modified reactions, the ratio of reagents is 12:1:1:159; $Na:(Nb + M^{IV}):L:H_2O$. The ligands alter the pH of the reaction mixture minimally. The Teflon liner containing the aqueous mixture is placed inside the steel pressure reactor, which is placed in a 175 °C oven for 4 h to 7 days. The yield of a typical reaction is approximately 0.4 g, or 90% yield based on the metal alkoxides.

General Instrumentation. X-ray Powder Diffraction (XRPD). X-ray powder diffraction data were collected on variable composition, Ti- and Zr-SOMS samples to determine unit cell parameters by Rietveld refinement. The powder data for the 2% Ti-SOMS were collected, and the National Synchrotron Light Source, Brookhaven National Laboratory (NSLS, BNL) XRPD data were collected at 298 K on the beamline X3B1 of NSLS at BNL. X-rays of wavelength approximately 0.700211 Å were selected by a double crystal Si (1 1 1) monochromator. The sample was mounted on the horizontal axis of the diffractometer. The

(15) Nyman, M.; Tripathi, A.; Parise, J. B.; Maxwell, R. S.; Harrison, W. T. A.; Nenoff, T. M. *J. Am. Chem. Soc.* **2001**, *123*, 1529.
(16) Johnson, G. M.; Reisner, B. A.; Tripathi, A.; Corbin, D. R.; Toby, B. H.; Parise, J. B. *Chem. Mater.* **1999**, *11*, 2780.
(17) Lee, Y.; Kim, S.-J.; Schoonen, M. A. A.; Parise, J. B. *Chem. Mater.* **2000**, *12*, 1597.
(18) Johnson, G. M.; Tripathi, A.; Parise, J. B. *Microporous Mesoporous Mater.* **1999**, *28*, 139.
(19) Nicolas-Tolentino, E.; Tian, Z.; Zhou, H.; Xia, G.; Suib, S. L. *Chem. Mater.* **1999**, *11*, 1733.
(20) Luo, J.; Zhang, Q.; Huang, A.; Giraldo, O.; Suib, S. L. *Inorg. Chem.* **1999**, *38*, 6106.
(21) Luo, J.; Zhang, Q.; Suib, S. L. *Inorg. Chem.* **2000**, *39*, 741.
(22) Rocha, J.; Anderson, M. W. *Eur. J. Inorg. Chem.* **2000**, 801.
(23) Anthony, R. G.; Dosch, R. G.; Phillip, C. V. U.S. Patent 6,110,378, Method of Using Novel Silico-titanates, Sandia National Laboratories, U.S.A., August, 2000.

diffracted X-rays are selected by a Ge (1 1 1) analyzer crystal on a detector arm and detected using a commercial NaI scintillation counter. The measured X-ray counts are normalized to the signal from an ionization chamber between the monochromator and sample in order to correct for decay and fluctuations of the incident beam intensity. All other X-ray powder patterns were generated at Sandia National Laboratories on a Siemens D500 diffractometer with Ni-filtered Cu Kα radiation. The data were collected over the angular range 5−90° 2θ with a step size of 0.04° and a counting time of 40 s per step. The front-loaded samples were rotated at 30 rpm during the measurement. **Variable Temperature X-ray Diffraction.** The mechanism of transformation from SOMS-1 to perovskite was investigated by using in situ dehydration studies. An imaging plate detector (Mar345, 2300 × 2300 pixels) was coupled to an in situ dehydration cell[24] at the X7B beamline of the NSLS. A powdered sample of SOMS-1 (~0.003 g) was loaded into a 0.3 mm quartz capillary, which was connected to a vacuum pump (<20 mTorr). A horseshoe-shaped heater[25] was placed close to the sample position. A continuous heating rate of 3 °C/min was used with an exposure time of 60 s for each frame without slits. The wavelengths (0.9379 Å), sample to detector distance, zero point, and IP tilt were determined using a LaB_6 standard (NIST SRM 660a) prior to the experiment. The temperature was calibrated using the known thermal expansion of an Ag standard. Data were integrated using the FIT2D suite of programs.[26] A 30° portion of Debye−Scherrer rings perpendicular to the plane of the orbit was chosen for integration since the divergence of the X-ray source is least in this direction. Thermogravimetric analysis−differential thermal analysis (TGA-DTA) experiments were performed on a STD 2960 TA DTA-TGA instrument with alumina as a standard for DTA. Samples (10−15 mg) were heated at 10 °C/min to 900 °C, and argon was used as a sweep gas with a flow of 20 cm^3/min. ^{1}H Magic angle spinning nuclear magnetic resonance (MAS NMR) experiments were performed at 300.1 MHz on a Chemagnetics CMX-300 spectrometer equipped with a 4 mm Bruker CPMAS probe. Spinning speeds between 4 and 12 kHz were employed with a 4 μs observe pulse and 10 s recycle delay. Chemical shifts were referenced to an external sample of tetramethylsilane (TMS, 0 ppm). ^{23}Na MAS NMR experiments were performed on a Bruker DRX-500 at 132.3 MHz at spinning speeds of 10−14 kHz. Chemical shifts were referenced to 0.1 M NaCl. A 2 s recycle delay and a 1 μs, π/10, pulse length were employed for excitation before data acquisition. Variable recycle delay experiments for both ^{1}H and ^{23}Na MAS NMR experiments were performed to ensure equilibration of magnetization. Infrared spectra (IR) were collected on a Perkin-Elmer SpectrumGX FT-IR instrument in the mid-IR range of 370−7000 wavenumbers operated in the transmittance mode. Samples for IR were prepared by mixing 1−3 wt % SOMS in a KBr (predried at 50 °C) matrix and pressed to form a disk. Compositions of SOMS were determined by ICP-MS spectroscopy at Galbraith Laboratories, Knoxville TN. SOMS samples were digested in hydrofluoric acid and diluted with deionized water. Weight percents of Na, Nb, and Ti or Zr were determined from ppm analyses of these samples. Scanning electron microscopy (SEM) data were collected on a JEOL JSM-T300 SEM with energy dispersive (EDS) capabilities. Samples were mounted on a graphite carbon disk and carbon coated (for EDS analysis). Samples for Raman spectroscopy were loosely packed in to a pellet holder and illuminated with a laser beam of 514 wavelength over an area of approximately 2 mm by 0.1 mm. Light was collected in backscatter configuration and dispersed and detected by a spectrograph and charge-coupled device.

Distribution Coefficient (K_d) Measurements. SOMS selectivity for Sr was measured as a function of pH, Na-concentration, and SOMS composition. In these selectivity experiments, $NaNO_3$, HNO_3, and NaOH were used to produce Na-containing solutions, acidic solutions, and basic solutions, respectively. Solutions were prepared with 50 ppm $Sr(NO_3)_2$. Ten milliter solutions were combined with 0.05 g of SOMS in 30 mL polypropylene bottles. The mixtures were capped and shook at 200 rpm at room temperature on a rotary shaker for 4 h. After contacting the SOMS, solutions were filtered and analyzed for Sr. The Sr analyses were carried out by Galbraith Laboratories, Inc. (Knoxville, TN) using inductively coupled plasma mass spectroscopy (ICP-MS). Distribution coefficient were calculated by the following relationship:

$$K_d\ (\mathrm{mL/g}) = ([\mathrm{Sr_{ix}}]/g_{ix})/([\mathrm{Sr_{sln}}]/\mathrm{mL\ sln}) \quad (1)$$

where K_d is the distribution coefficient, ix is ion exchanger, $[Sr_{ix}]$ is the concentration of Sr adsorbed by the ion exchanger, g_{ix} is the weight of the SOMS ion exchanger, $[Sr_{sln}]$ is the concentration of the Sr remaining in solution after contacting SOMS, and mL sln is milliliters of solution.

Results and Discussion

Synthesis. The reaction procedures described above in the Experimental Section produced SOMS-1 structural analogues of varying Nb:M^{IV} ratios. The large quantity of NaOH (33.6 mmol, 1.34 g) used in the syntheses aid in producing pure crystalline material, with no amorphous byproducts. The pH of >13.5 of these reactions can be achieved with half the amount of NaOH (~17 mmol, 0.67 g), but higher NaOH concentrations yielded a purer product, perhaps due to more complete solvation of the precursors.

In the course of this work, two synthetic challenges arose in our efforts to obtain suitable SOMS materials for single-crystal and bulk analyses. The first was to obtain crystals larger enough for Synchrotron data collection on a single crystal. This was accomplished with the Ti-SOMS series. A reaction of 1:4 Ti:Nb (the maximum Ti:Nb ratio possible to obtain pure phase SOMS) produced needlelike crystals with preferential growth along the *b*-axis and aspect ratios up to 50:1. Increasing the ratio of Ti:Nb up to 2:1 in the reaction mixture produced larger SOMS-1 (1:4 Ti:Nb ratio) crystals with a more rectangular morphology (plus an amorphous, titania-rich material as a byproduct). The resulting increase in crystal size and decrease in aspect ratio with increasing Ti in the reaction mixture is observed in series of scanning electron micrographs in Figure 1.

However these SOMS crystals have a tendency toward 180° rotational twinning along the *b*-axis, and therefore the structure solution was further complicated by the effects of this twinning.[15,27] The twinned faces of SOMS crystals can be clearly observed in the micrograph in Figure 2.

The second synthetic challenge was obtaining pure-phase SOMS materials with M^{IV}:Nb (M = Ti, Zr) ratios less than 1:4, so that systematic bulk characterizations could be carried out. The Ti-SOMS reaction mixtures tended to form the very stable orthorhombic $NaNb_{1-x}Ti_xO_3$ perovskite (JCPDS #73-0803), and the likelihood of perovskite formation was greater with lower concentration of alkoxide Ti^{IV} precursor in the reaction mixture. The precursor mixtures for Zr-SOMS tended to produce impurities in the form of either the perovskite phase or hexagonal $NaNb_{1-x}Zr_xO_3$ illmenite with a = 5.3403(7) Å and c = 15.620(3) Å. Formation of these undesired condensed

(24) Lee, Y.; Reisner, B. A.; Hanson, J. C.; Parise, J. B.; Corbin, D. R.; B. H. Tody, A. F.; Larese, J. Z.; Kahlenberg, V. *J. Phys. Chem.* **2001**, *105*, 7188.
(25) Brown, G. E.; Sueno, S.; Prewitt, C. T. *Am. Mineral.* **1973**, *58*, 698.
(26) Hammersley, A. P. *FIT2D: V9.129 Reference Manual V3.1*, 1998.
(27) Tripathi, A.; Nyman, M.; Nenoff, T. M.; Parise, J. B.; Harrison, W. T. A. Structure of $Na_{16}(Nb_{12.8}Ti_{3.2})O_{44.8}(OH)_{3.28}H_2O$, a selective ion exchanger for sequestration of Sr^{2+}, from a twinned 5 x 8 x 8 m^3 crystal using synchrotron X-ray radiation source. American Crystallographic Association Meeting, St. Paul, MN, July 21−27, 2000.

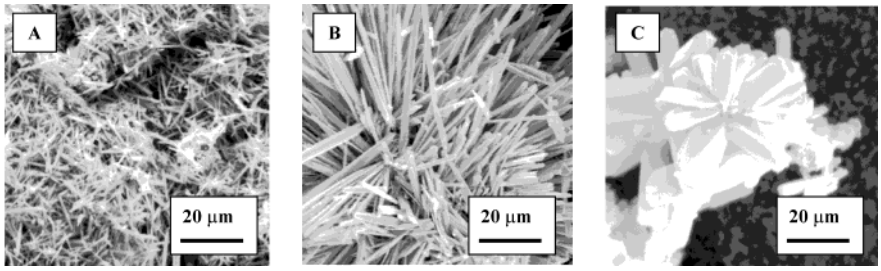

Figure 1. Scanning electron micrograph images of 20% Ti-SOMS ($Na_2Nb_{1.6}Ti_{0.4}O_{5.6}(OH)_{0.4}\cdot H_2O$) synthesized with varying Nb:Ti ratio in the alkoxide precursor mixture, illustrating morphology change with increasing titanium in the reaction mixture. (a) Nb:Ti = 4:1, (b) Nb:Ti = 1:1, (c) Nb:Ti = 1:2.3.

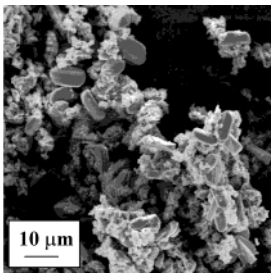

Figure 2. Scanning electron image of 20% Ti-SOMS ($Na_2Nb_{1.6}Ti_{0.4}O_{5.6}(OH)_{0.4}\cdot H_2O$) used for synchrotron data collection. The rotational twinning plane along the *b*-axis is visible in these crystals.

phases was particularly pronounced for the synthesis of the Zr-SOMS, either due to the lower solubility of zirconium dioxide in the reaction solution or the greater size "misfit" between the disordered metals: Zr^{IV}(0.84 Å) and Nb^{V}(0.78 Å) compared to Ti^{IV} (0.75 Å) and Nb^{V}.[28] Both the addition of ligands such as 2,4-pentadione and peroxides and shorter reaction times aided in obtaining pure-phase SOMS. The ligands, which were chosen due to their affinity to binding Ti and Zr, likely aid SOMS formation by increasing dissolution of the relatively (compared to Nb) insoluble oxides of Ti and Zr in the basic, aqueous reaction mixtures. Without sufficient concentrations of Ti or Zr in solution to form the metastable SOMS phase, the more stable $NaNb_{1-x}M^{IV}_xO_3$ perovskite or illmenite formed. Reaction time also affected the products that formed. For instance, in one series of Ti-SOMS syntheses, the reaction product went from predominantly SOMS with minor hexaniobate[29,30] (JCPDS #84-188; $Na_7(H_3O)(Nb_6O_{19})(H_2O)_{14}$), to pure SOMS, to SOMS with minor perovskite, to predominantly perovskite with minor SOMS as the reaction time was increased from 4 to 16 h.

The hydrogen peroxide was both advantageous and disadvantageous in the role of SOMS formation. Hydrogen peroxide aided in SOMS formation by increasing the solubility of M^{IV}, but also aided in SOMS decomposition by extracting the M^{IV} from the framework. This was observed by formation of a yellow solution in SOMS synthesis experiments containing hydrogen peroxide (indicative of hydrogen peroxide binding to Ti in solution). The *tert*-butylhydroperoxide, however, favored Ti-SOMS formation without simultaneous decomposition of the SOMS. This is likely due to the poorer binding ability of the *tert*-butylhydroperoxide compared to hydrogen peroxide, or the increased difficulty of the larger amphiphilic molecule to penetrate the water-filled pores of SOMS.

The Zr-SOMS afforded its purest product with a reaction time of around 24 h and with hydrogen peroxide as a solubility-aiding ligand. The 2,4-pentadione, while useful in aiding in both Zr- and Ti-SOMS formation, tended to decompose to form dark-colored organic material which was difficult to remove from both SOMS powders and Teflon reaction vessels. In Table 1 is summarized the product(s) formed from 1:9 Ti:Nb precursor mixtures, showing the effects of reaction time and ligand on product obtained, summarizing the importance of these synthesis parameters on SOMS formation.

Table 1. Product(s) Obtained from 12:0.1:0.9 Na:Ti:Nb Reaction Mixtures

experiment	reaction time	ligand	product
1	12 h	none added	major perovskite, trace SOMS
2	12 h	hydrogen peroxide	major SOMS, minor perovskite
3	12 h	*tert*-butylhydroperoxide	SOMS
4	12 h	2,4-pentadione	major SOMS, minor amorphous
5	4 days	hydrogen peroxide	major perovskite, minor SOMS
6	4 h	hydrogen peroxide	SOMS plus hexaniobate
7	4 h	none added	major SOMS plus minor hexaniobate

Structural and Compositional Characterization of SOMS. The structure of SOMS-1, $Na_2Nb_{1.6}Ti_{0.4}O_{5.6}(OH)_{0.4}\cdot H_2O$, was determined from single-crystal X-ray diffraction data collected at NSLS, BNL, and described in detail previously.[15] Briefly, the framework consists of layers of edge-sharing sodium octahedra parallel to the *xy* plane, interleaved with double chains of edge-sharing, distorted Nb/M^{IV} octahedra running along the *b*-axis. The distorted, square-planar sodium is located within channels running parallel to the *b*-axis, between the Nb/M^{IV} octahedra chains, and is bonded to two water molecules (Ow) and two framework oxygens (O4). The two Nb/M^{IV} sites are completely disordered and distorted. Each site has one long (~2.4 Å) and one short (~1.8 Å) axial Nb/M^{IV} −O bond, as well as displacement of Nb/M^{IV} above the equatorial plane. The equatorial Nb/M^{IV} −O bonds are all ~2 Å, but the displacement of above the equatorial plane gives rise to trans O− Nb/M^{IV} −O bond angles as small as 147 °. The $Nb/M^{IV}1$ site is shown in Figure 3, illustrating the modes of distortion. Raman spectroscopy also confirmed these two types of octahedral distortion; with peaks at 374, 460, 771, and 884 cm^{-1} for the axial distortion and peaks at 305, 638, and 844 cm^{-1} for the equatorial plane distortion.[31]

A series of SOMS analogues with variable $Nb:M^{IV}$ (for both M = Ti, Zr) compositions were synthesized and characterized

(28) Shannon, R. D. *Acta. Crystallogr.* **1976**, *A32*, 751.
(29) Tobias, R. S. *Can. J. Chem.* **1965**, *43*, 1222.
(30) Muller, M. *Revue de Chimie minerale* **1970**, *7*, 359.
(31) Jehng, J. M.; Wachs, I. E. *Chem. Mater.* **1991**, *3*, 100.

Table 2. Unit Cell Parameters as a Function of SOMS Composition

% M^{IV} [a]	*a*, Å (esd)	*b*, Å (esd)	*c*, Å (esd)	β, deg (esd)	vol, Å^3 (esd)	R_{Bragg} (%)
20% Ti	16.940(3)	5.033(5)	16.466(3)	114.00(3)	1282.6(3)	6.87 (single crystal)
12.5% Ti	16.8906(3)	5.0381(6)	16.456(2)	114.002(5)	1279.2(3)	8.21
10.3% Ti	16.965(3)	5.0256(8)	16.464(3)	113.984(6)	1282.5(4)	7.65
14.9% Ti	16.928(2)	5.0296(5)	16.461(2)	113.983(4)	1280.5(2)	6.41
6.7% Ti	16.940(2)	5.0229(7)	16.477(2)	113.956(5)	1284.9(3)	7.36
2.0% Ti	16.936(3)	5.0277(6)	16.459(3)	113.972(5)	1283.6(3)	7.52
16.7% Zr	17.065(2)	5.0408(9)	16.514(2)	113.997(6)	1297.6(4)	8.38
12.5% Zr	17.042(2)	5.0217(9)	16.473(2)	114.015(5)	1287.5(3)	7.85
5.3% Zr	17.051 (2)	5.0348 (8)	16.510 (2)	113.983 (5)	1294.9 (3)	7.64
2.9% Zr	17.062 (2)	5.040 (8)	16.523 (2)	113.974 (5)	1298.2 (3)	6.43
1.6% Zr	17.03778 (5)	5.0314 (2)	16.4877 (5)	113.972 (2)	1291.48 (7)	9.66

[a] The amount of M^{IV} substituted into the nominal Nb^V sites, as determined by bulk chemical analysis.

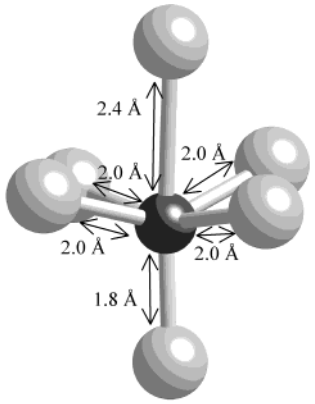

Figure 3. Ball and stick representation of the Nb/M^{IV}1 distorted octahedral site, illustrating the geometry of the distortion (identical distortion is observed for the Nb/M^{IV}2 site).

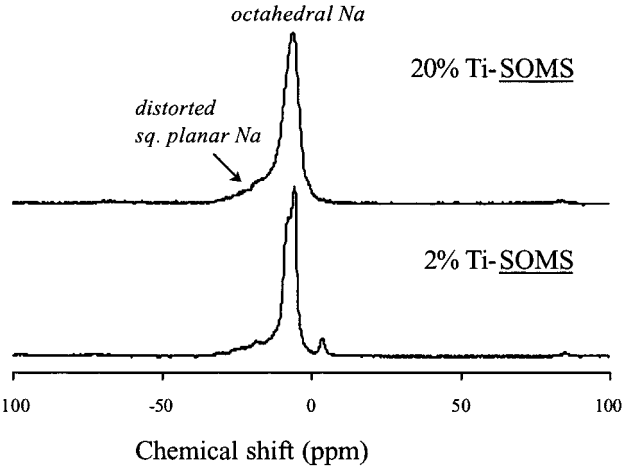

Figure 4. ^{23}Na MAS NMR spectra for 2% Ti-SOMS (bottom) and 20% Ti-SOMS (top). Both SOMS compositions have a 3:1 octahedral (−8 ppm) to square-planar (−11 ppm) sodium ratio, which illustrates the sodium composition does not change with changing Nb:M^{IV} ratio. The relative broadening of the 20% Ti-SOMS peaks is due to increasing disorder in the second coordination sphere with increasing Ti substitution on the Nb/M^{IV}1 and Nb/M^{IV}2 sites. The small sharp peak at 3.3 ppm in the 2% Ti-SOMS spectrum is a minor perovskite impurity.

to determine how the M^{IV} substitution of the framework is charge-balanced by cations. The most logical possibilities for charge-balancing the M^{IV}-substitution of the framework are by population of the Na3 square planar site in the channels (one Na3 added for each M^{IV} substituted) or by addition of an H^+ for each M^{IV} substituted into the framework. In fact, all spectroscopic evidence confirmed addition of an H^+ for each M^{IV} as a mechanism of charge-balancing the framework, which is reflected in the general formula we have defined for SOMS, $Na_2Nb_{2-x}M^{IV}_xO_{6-x}(OH)_x\cdot H_2O$ (M^{IV} = Ti, Zr; $x = 0.04-0.40$). Within the following paragraphs, these spectroscopic studies are described.

Several methods were used to characterize the cation sites in the series of variable composition SOMS materials. Bulk chemical analyses (by Galbraith Laboratories, Inc.) revealed that the sodium content does not increase with increasing M^{IV}. Further, Rietveld refinements of SOMS materials with variable Nb:M^{IV} ratios were carried out by using the structure of SOMS-1 as a model (see Table 2). In these refinements, the Na3 population was allowed to vary; and for each composition, this site refined to a fully occupied state. Similarly, ^{23}Na MAS NMR experiments showed a consistent ratio of octahedral to square-planar Na coordination sites of approximately 3:1, as predicted by the structure, for all compositions. The ^{23}Na MAS NMR spectra of 20%Ti-SOMS (SOMS-1) and 2%Ti-SOMS are shown in Figure 4. Two peaks are apparent: the relatively narrow octahedral Na peak at -8 ± 1 ppm (Na1[8 per unit cell] plus Na2 [4 per unit cell]) and the significantly broader square-planar Na3 peak at -11 ± 2 ppm (4 per unit cell). Although the ratios of these peaks are the same between minimum (2%) and maximum (20%) titanium substitution, the spectra of the 2%Ti-SOMS shows better-defined, narrower peaks. This peak-sharpening is likely due to the increased disorder on the Nb/Ti1 and Nb/Ti2 framework sites in the second coordination sphere of the Na sites with increasing Ti. Octahedral Na1 bridges Ti/Nb sites through five of its oxygen bonds, octahedral Na2 bridges Ti/Nb sites through all six of its oxygen bonds, and distorted square-planar Na3 bridges Ti/Nb sites through two of four of its oxygen bonds. The Na1 is bonded to water through its sixth bond, and Na3 is bonded to water through two of four of its bonds.

A comparison of the ^{1}H MAS NMR spectra (Figure 5) of a high (20%) and low (2%) concentration Ti gave direct evidence for addition of protons on two distinct oxygen sites that accompanies and charge-balances each substitution of a Ti into a framework Nb site. As observed in Figure 5, the SOMS has two sites for protons (evidenced by the two hydroxyl peaks in the 20% Ti-SOMS ^{1}H spectrum), and the occupancy of these sites increase with increasing Ti-substitution into the framework. Both ^{1}H NMR spectra have the water peak at 4.3 ppm and an O−H peak at ∼1 ppm. The 20% Ti-SOMS has an additional acidic O−H peak around 7 ppm, which is not observed in the 2% Ti-SOMS. The ratio of water peak at 4.3 ppm to the OH peak at 1 ppm is around 97:3 for the 2% Ti-SOMS which corresponds adequately with the predicted formula of $Na_2Nb_{1.96}M^{IV}_{0.04}O_{5.96}(OH)_{0.04}\cdot H_2O$ (98% water, 2% OH). In the

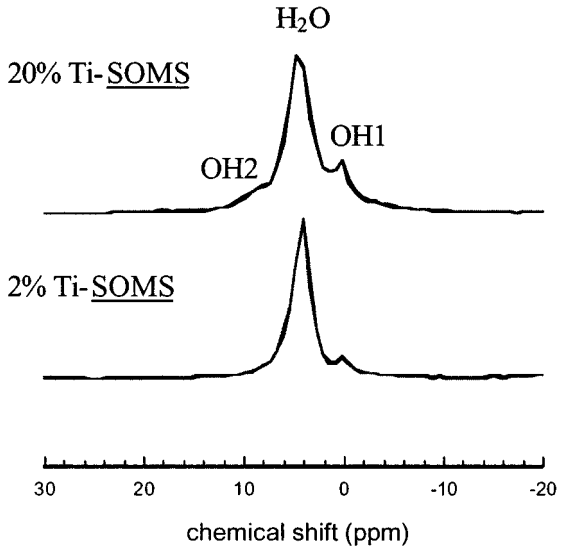

Figure 5. ^{1}H MAS NMR spectra for 2% Ti-SOMS and 20% Ti-SOMS, showing increase in O−H groups with increasing Ti-substitution on the Nb/M^{IV}1 and Nb/M^{IV}2 sites.

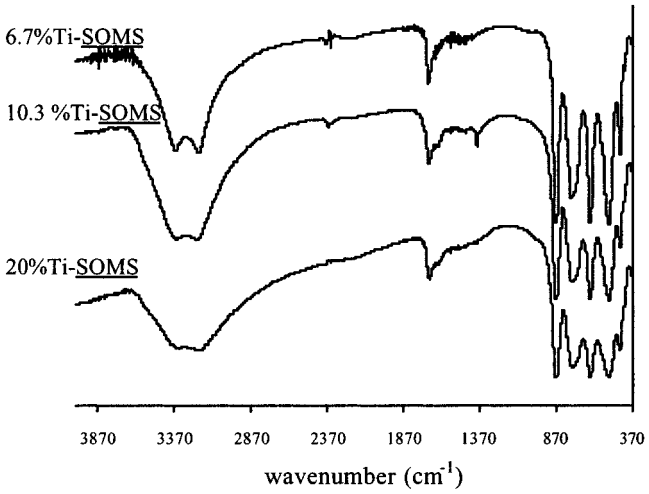

Figure 6. Mid-IR spectra of 5%, 10%, and 20% Ti-SOMS showing increased broadening of both the O−H vibrational bands and metal−oxygen framework vibrational bands, indicating increased H-bonding and increased substitution of Ti^{IV} into the framework, respectively.

20% Ti-SOMS, the peaks are 78% H_2O:15% OH (1 ppm):7% OH (7 ppm). Again this corresponds reasonably well with the predicted formula: $Na_2Nb_{1.6}M^{IV}{}_{0.4}O_{5.6}(OH)_{0.4}\cdot H_2O$ (84% water, 16% OH). The acidic peak at 7 ppm is broad, likely due to hydrogen bonding (bridging) to another framework oxygen or water oxygen, which is also observed by the broadening of the IR, O−H vibrational bands of the 20% Ti-SOMS (see below).[32]

Infrared spectroscopy also gave evidence for the presence of increasing H-bonded O−H groups within the pores, as well as increased disorder on the Nb/M^{IV} sites with increasing M^{IV} substitution. Figure 6 shows the mid-IR spectra of 5% Ti-SOMS, 10% Ti-SOMS, and 20% Ti-SOMS. Although all samples are well-crystallized, we see an increased broadening in vibration bands with increasing Ti substitution. This is particularly true in the adsorption band of the O−H stretch in the region between 2800 and 3500 cm^{-1}. The adsorption peak around 1600 cm^{-1} is the H−O−H bend of the molecular water bonded to the Na3 and Na1 sites. As expected, this adsorption band does not change with changing Ti framework concentration, since these sites do not change in occupancy or composition as the framework Nb/Ti ratio changes. The adsorption bands below 1000 cm^{-1} are vibrations of the Na-titanoniobate framework including M−O stretching, M−O−M bending (M = Ti, Nb, Na), and lattice vibrations. These also exhibit broadening with increasing Ti incorporation into the lattice. The broadening of the O−H stretch at 2800−3500 cm^{-1} is indicative of hydrogen bonding,[33] which is consistent with the ^{1}H NMR results where we see an increase in acidic protons (made acidic by H-bonding) with increasing M^{IV}. However, we do not see a significant increase in the intensity of this band with increasing O−H. This is probably because this signal is dominated by water. Given the general formula for SOMS, $Na_2Nb_{2-x}M^{IV}{}_xO_{6-x}(OH)_x\cdot H_2O$, the ratio of water O−H bonds to hydroxyl O−H bonds is 20:1 for the 5% Ti-SOMS and 5:1 for the 20% Ti-SOMS. The broadening of the adsorption bands of the lattice vibrations (below 1000 cm^{-1}) with increasing substitution of Ti on the Nb framework sites may be a result of increased disorder, or decreased symmetry of the lattice sites, and the decreased symmetry results in broadening of the adsorption band of each vibrational frequency.[34] The broadening of the IR spectra with increasing Ti-substitution is also consistent with the broadening of the ^{23}-Na NMR spectra, as the disorder on the Nb/M^{IV} framework sites increases.

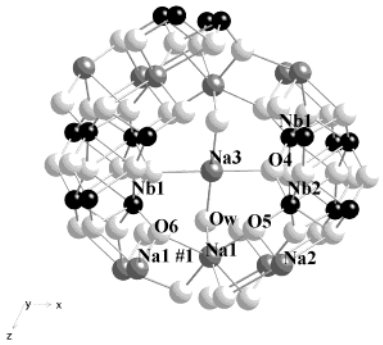

Figure 7. A view of the SOMS pore containing distorted square-planar Na3. The O4 and O6 sites are the most likely sites for binding of the charge-balancing protons, due to the bond angle changes and bond length changes observed around these oxygen sites with increasing substitution of Ti^{IV} into the framework (see Table 3).

According to ^{1}H NMR results, there are two unique sites for charge-balancing protons, and the siting of these protons is most reasonably placed on the O4 and O6 oxygens which frame the channels containing Na3 (see Figure 7). The siting of protons in aluminosilicate zeolite frameworks has been a topic of extensive study, due to the catalytic reactivity of these sites. A combination of theoretical and experimental studies have shown that protonated sites of zeolites have decreased M−O−M (M = Si, Al) bond angles and increased M−O bond distances, compared to their deprotonated counterparts.[35,36] In the aluminosilicate tetrahedral frameworks, all framework oxygens bridge two corner-sharing tetrahedra. In the octahedral SOMS frame-

(32) Freude, D. *Chem. Phys. Lett.* **1995**, *235*, 69.
(33) Nakamoto, K. *Infrared and Raman Spectra of Inorganic and Coordination Compounds*; John Wiley & Sons: New York, 1978.
(34) Gonzalez-Hernandez, J.; Perez-Roblez, J. F.; Espinoza-Beltran, F. J.; Garcia-Rodriguez, F. J.; Vorobiev, Y. V.; Yanez-Limon, M.; Garcia-Cerda, L. A. *Inorg. Mater.* **1998**, *34*, 1275.
(35) Sierka, M.; Eichler, U.; Datka, J.; Sauer, J. *J. Phys. Chem. B* **1998**, *102*, 6397.
(36) Eichler, U.; Brandle, M.; Sauer, J. *J. Phys. Chem. B* **1997**, *101*, 10035.

Table 3. M−O−M Bond Angles and M−O Bond Lengths (M = Na, Ti/Nb; O = O4, O5, and O6)[a]

M–O-M (M = Na, Ti/Nb)	2% Ti-SOMS angle (deg)	20% Ti-SOMS angle (deg)	bond	2% Ti-SOMS bond length (Å)	20% Ti-SOMS bond length (Å)
Nb1−O4−Nb2 #4	134.0 (4)	118.8 (3)	Nb1−O4	1.848 (7)	1.962 (8)
Nb2 #4-O4−Na3 #15	107.7 (3)	105.6 (7)	Nb2−O4	1.865 (8)	1.997 (8)
Nb1−O4−Na3 #12	118.3 (7)	118.7 (7)	Na3−O4	2.48 (4)	2.25 (3)
Nb2−O5−Na2	102.7 (8)	103.8 (4)	Nb2−O5	2.018 (9)	1.809 (8)
Na1 #16-O5−Na2	107.9 (2)	99.9 (3)	Na1−O5	2.296 (8)	2.413 (9)
Nb2−O5−Na1 #16	127.4 (3)	132.0 (5)	Na2−O5	2.230 (8)	2.351 (9)
Nb1−O6−Na1	117.6 (1)	100.3 (3)	Nb1−O6	1.731 (8)	1.802 (7)
Na1−O6−Na1 #17	115.4 (5)	114.1 (3)	Na1−O6	2.69 (1)	2.555 (9)
Nb1−O6−Na1 #17	118.6 (3)	131.1 (5)	Na1−O6	2.69 (1)	2.555 (9)

[a] Symmetry transformations used to generate equivalent atoms: #4, $-x+1, -y+1, -z+2$; #12, $-x+1/2, -y+1/2, -z+1/2$; #15, $x, y, z+1$; #16, $-x+1, y+1, -z+3/2$; #17, $-x+1/2, y+1/2, -z+3/2$.

works, the framework oxygens bridge three octahedral or distorted square-planar sites, which may be edge-sharing or corner-sharing. Given the more complex nature of the oxygen sites within the SOMS framework, a direct correlation between structural parameters and protonation cannot be so easily drawn out. However, the narrative below, along with the structural data compiled in Table 3 gives evidence to support our proposed proton sitings of O4 and O6.

Table 3 lists the M−O−M bond angles and M−O bond lengths (M = Nb/Ti, Na) around the O4, O5, and O6 sites for the 2% and 20% Ti-SOMS. The Nb/Ti−O bonds lengthen on the O4 and O6 sites with protonation of the SOMS framework and decrease on the O5 site. The Nb/Ti−O−M (M = Na, Nb/Ti) angles decrease on the O4 and O6 site with protonation of the SOMS framework and increase slightly on the O5 site. This is analogous to the behavior of the aluminosilicate frameworks and consistent with protonation of the O4 and O6 sites. However, the Na−O bond lengths exhibit anomalous behavior by decreasing on the O4 and O6 with protonation of the SOMS framework and increasing on the O5 site. This may be explained by the electronegativity differences between Nb^{V}/Ti^{IV} and Na^{I}. Ti^{IV} and Nb^{V} have similar electronegativities and are more electronegative than Na^{I},[37] and therefore are more likely to be affected by the change in polarization of the electron density on the oxygen in response to protonation. Hence, the Na−O bonds, which are not extremely affected by polarization of oxygen, shorten in response to geometric constraints that are imposed by the lengthening of the Nb−O bonds. Similarly, the perturbations of the O5 geometry may be in response to framework distortions caused the proton-induced changes on the O4 and O6 sites.

The geometry of the O4, O5, and O6 sites is shown in the polyhedral representation in Figure 8. This figure shows the following: (1) The O4 is bonded to M1, M2 (M = M^{IV}/Nb), and Na3; the M1 and M2 are edge-sharing and the Na3 is corner-sharing with both M1 and M2. (2) Similarly, the O6 is bonded to two Na1 sites and M1; the M1 and one Na1 are edge-sharing and the second Na1 is corner-sharing with both M1 and the first Na1. (3) However, O5 is bonded to Na1, Na2, and M1; Na1 and Na2 are edge-sharing and Na2 and M2 are edge-sharing. This geometry of the O5 site gives it less flexibility to undergo bond angle distortions to accommodate a proton, compared to the less rigid O4 and O6 sites, which may be the ultimate reason the O4 and O6 sites are protonated, rather than the O5 site.

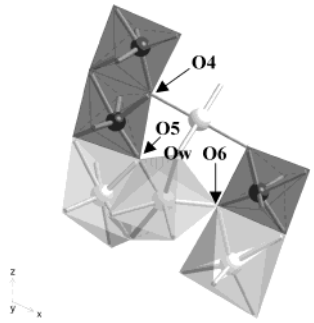

Figure 8. Polyhedral representation of the SOMS framework emphasizing the binding geometry of the O4, O5 and O6 sites. The O5 site is the most "rigid", surrounded by three edge-sharing polyhedra. The O4 and O6 sites are less rigid, in that they are surrounded by both corner-sharing and edge-sharing polyhedra.

We also carried out Rietveld refinement of the X-ray powder diffraction data for the variable composition Ti- and Zr-SOMS to determine if altering the composition resulted in a change in the unit cell parameters. The compositions and unit cell parameters for a series of SOMS materials are compiled in Table 2, where compositions were determined by bulk chemical analyses. These studies showed that for the Ti-SOMS there is very little change in unit cell parameters with changing Ti concentration. Further, the unit cell changes do not scale with composition. This is likely because (1) there is only 5% difference between the radii of Ti and Nb (octahedral Ti^{IV} radius = 0.75 Å, octahedral Nb^{V} radius = 0.78 Å[28]) and (2) the framework is flexible enough to accept the increase in protons within the pores with increasing M^{IV} concentration, and therefore only slightly distorts the framework. In contrast, the Zr-SOMS show a slight increase in unit cell volume, likely because there is a larger size difference between Nb and Zr. However, volume does not scale with increasing Zr^{IV} substituted into the framework (radius of octahedral Zr^{IV} = 0.86 Å[28]).

Thermal Stability of SOMS. Thermogravimetric analysis−differential thermal analysis (TGA-DTA) of variable composition, Ti- and Zr-SOMS provided information on the thermal stability of SOMS as a function of composition. Figure 9 shows the TGA-DTA spectra of Ti-SOMS and Zr-SOMS, respectively. All SOMS compositions have two weight loss events upon heating. The weight loss between 150 and 250 °C is the loss of framework water and hydroxyls, which varies from 7 to 8.5 wt % for the range of SOMS compositions synthesized. Below 150 °C is likely surface water, which may vary in quantity, depending on the method of sample preparation and surface area of the particular sample. There is no further weight loss up to 900 °C. Observation of the DTA curve shows both the

(37) Allred, A. L. *J. Inorg. Nucl. Chem.* **1961**, *17*, 215.

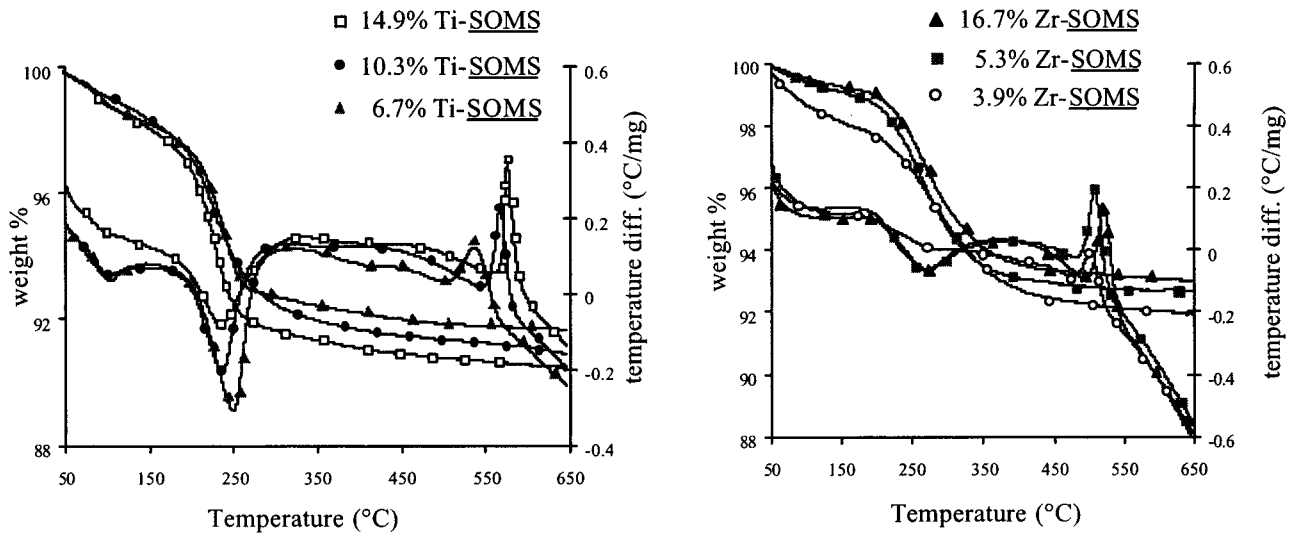

Figure 9. (a) TGA-DTA spectra of 6.7%, 10.3%, and 14.9% Ti-SOMS and (b) TGA-DTA spectra of 3.9, 5.3, and 16.7% Zr-SOMS. Both show increased weight loss with increasing framework M^{IV}, due to the corresponding increase in charge-balancing protons. The temperature of conversion to perovskite *increases* with increasing Ti in the framework, and the temperature of conversion to perovskite *decreases* with increasing Zr in the framework (see also, Table 4).

endothermic loss of water and hydroxyls, and an exothermic event that occurs between 500 and 600 °C. This exotherm corresponds with conversion of the SOMS framework to a perovskite structure. The temperature of perovskite formation varies with SOMS composition; increasing temperature with increasing Ti^{IV} and decreasing temperature with increasing Zr^{IV}. These results suggest that Ti^{IV} stabilizes the SOMS structure, while Zr^{IV} destabilizes the SOMS structure. The "stabilization" of SOMS with increasing Ti^{IV} in the framework (along with corresponding increase in OH content) may be due to the hydrogen bonding within the pores. The Zr-SOMS should also have increased H-bonding with increasing Zr^{IV}, but may be "destabilized" by the size mismatch between Nb^{V} and Zr^{IV}. Calorimetry studies (Navrotsky, U.C. Davis) are presently under investigation to further understand this phenomenon. We also investigated the effect of the atmosphere on thermal conversion of SOMS to perovskite. A comparison was made between TGA-DTA conversion of SOMS to perovskite using argon and oxygen. The presence of oxygen during SOMS conversion to perovskite may be pertinent because the M^{IV}-substitution in perovskites is presumably charge-balance by oxygen vacancies ($NaNb_{1-x}M^{IV}_xO_{1-0.5x}$). However, the decomposition of SOMS to perovskite appeared to not be affected by the presence of oxygen, in light of the TGA-DTA experiments, as well as X-ray analysis of the resultant decomposition product. The temperatures of perovskite formation as a function of composition for a series of Ti-SOMS and Zr-SOMS are summarized in Table 4.

To investigate the pathway of dehydration and thermal decomposition of SOMS, we carried out in situ, variable temperature X-ray diffraction of SOMS-1 at the NSLS. The X-ray diffraction patterns of SOMS-1 as a function of temperature are shown in Figure 10. In agreement with TGA-DTA studies, the conversion of SOMS to perovskite is quite rapid. Rapid formation of perovskite is indicated by the short duration for the perovskite peaks to appear and grow to maximum intensity (approximately 5 frames, or 5 min) in the variable temperature XRD experiments and the sharp exothermic peak in the TGA-DTA experiments. The temperature of conversion

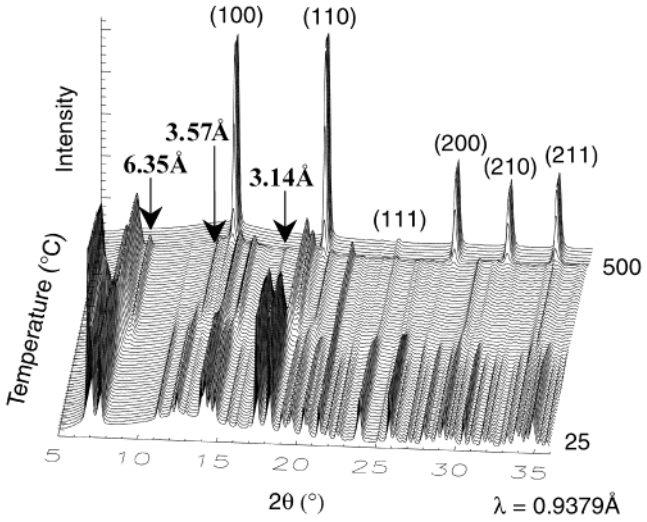

Figure 10. Plot of the synchrotron X-ray powder diffraction profiles as a function of time during the 5-h dehydration of SOMS-1 (20% Ti-SOMS). The marked peaks are characteristic of the intermediate phase, and do not overlap with peaks of either the SOMS or the perovskite.

Table 4. Temperature of Perovskite Formation for Variable Composition SOMS

SOMS composition (% M^{IV})	temperature of perovskite formation (°C)
6.7% Ti	538
10.3% Ti	568
14.9% Ti	575
20.0% Ti	576
1.6% Zr	532
3.9% Zr	521
5.3% Zr	509
16.7% Zr	501

of SOMS-1 to perovskite is around 500 °C in this experiment, compared to 576 °C in the TGA-DTA experiment. This difference is likely due to the difference in heating rate (3 °C/min for the in situ XRPD studies and 10 °C/min for the TGA-DTA studies). Finally, we note the formation of an intermediate phase formed between 300 and 450 °C, particularly indicated

by the peaks at $d = 6.35$, 3.57, and 3.14 Å which do not overlap with any diffraction peaks of either SOMS or perovskite. The temperature range at which this intermediate phase is predominant is bracketed by complete dehydration of SOMS-1 (indicated by TGA-DTA) and perovskite crystallization. This intermediate phase is only formed in vacuo, such as the conditions of this in-situ XRPD heating experiment. Structure determination of this intermediate phase between SOMS-1 and perovskite is currently under investigation.

Sr Selectivity of SOMS. Previously, we reported[15] SOMS selectivity for a variety of alkali, alkaline earth, and transition metals in 50 ppm, neutral solutions containing no competitive cations. In these scoping studies, it was determined that SOMS showed high selectivity for divalent metals and low selectivity for monovalent metals. We are currently investigating further the selectivity of SOMS for Sr^{2+} as a function of [Na] concentration, pH and SOMS composition. We are interested in Sr selectivity in particular since it is a prevalent α-emitter found in nuclear waste tanks,[39−41] as well as contaminated soils and groundwater surrounding these waste storage sites. Therefore, our more detailed selectivity studies were focused on Sr. The results and discussions that are given presently are to aid in the understanding of how compositional change (M^{IV} concentration) of SOMS affects its ion exchange properties.

Much evidence presented in this paper, as well as the initial Communication,[15] shows that the proton added to the SOMS framework for each Nb^{V}—M^{IV} (M = Ti, Zr) substitution is responsible for the divalent cation selectivity. The charge-balanced ion exchange takes place by

$$Na^{+}_{SOMS} + H^{+}_{SOMS} + Sr^{2+}_{solution} \rightarrow Sr^{2+}_{SOMS} + Na^{+}_{solution} + H^{+}_{solution} \quad (2)$$

where a divalent Sr in solution exchanges for a proton plus a sodium in the SOMS. We observed in the 20% Ti-SOMS that the maximum exchange capacity for Sr exactly matches that of the Ti concentration, which matches the framework OH concentration.[15] Further, the proton peaks in the ^1H NMR spectra of Sr-exchanged, 20% Ti-SOMS are much diminished (undetectable). Figure 11 shows Sr selectivity of 20% Ti-SOMS as a function of pH with 0.1 M Na, 0.01 M Na and no Na as a competitive cation (error on K_d values is 10%, or ± 5%). While it is difficult to compare K_d values to those of previous reports in that selectivity experiments are rarely done under identical conditions, a report by Behrens et al.[39] provided Sr selectivity studies comparable to the studies reported here. For these reported experiments and our [Na] = 0.1 M experiments, *V*:*m* (volume solution:mass ion exchanger) = 200, and ratio of Na:Sr ∼ 150. Behrens et al. reported Sr K_d values ranging from 5000−30000 for aluminosilicate zeolites, titanosilicates, germanium-substituted zeolites, and sodium titanate. These values are 1−2 orders of magnitude higher than comparable Sr K_d values for SOMS. Therefore, while SOMS exhibits superior Sr sorption while no competing cations are present, their performance suffers in the presence of an excess of other exchangeable cations.

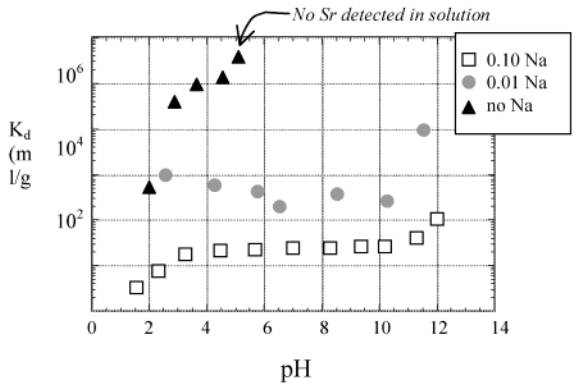

Figure 11. Selectivity (K_d, mL/g) of 20% Ti-SOMS for Sr as a function of pH and concentration of Na as a competing cation (error on K_d values is 10%, or ±5%).

The selectivity decreases with increasing [Na] concentration and increases with increasing pH. The increase in Sr selectivity with increased pH is consistent with this exchange mechanism. A basic aqueous medium (high pH) removes framework protons more easily than a lower pH solution. Finally, a comparison of the Sr selectivity of 20% Ti-SOMS with 2% Ti-SOMS in a solution of 0.1 M Na and 50 ppm Sr shows that 2% Ti-SOMS has a K_d of 98 mL/g and 20% Ti-SOMS has a K_d of 1723 mL/g.

Conclusions

Sandia octahedral molecular sieves (SOMS) encompassing Ti-SOMS and Zr-SOMS types is a variable-composition class of niobate-based ion exchangers. The framework composition, particularly the Nb:M^{IV} (M = Ti, Zr) ratio, influences the channel composition in two ways. First, we have shown the mechanism of charge-balancing the various composition analogues is proton addition. Second, we have shown that ion exchange occurs by exchange of a sodium plus a proton for a divalent cation, such as strontium. From TGA-DTA of the variable composition SOMS materials, we have learned the framework composition also affects the stability of the SOMS, by way of its temperature of thermal conversion to perovskite. Increasing Ti^{IV} concentration in the SOMS framework results in increased temperature of perovskite formation, and increasing Zr^{IV} concentration in the SOMS framework results in decreased temperature of perovskite formation. This corresponds with *increasing* SOMS stability with increasing Ti concentration, and *decreasing* SOMS stability with increasing Zr concentration. The instability of the Zr-SOMS is tentatively attributed to the larger "misfit" of the Zr^{IV} into the Nb^{V} framework sites, in that Zr^{IV} is considerably larger than Nb^{V}. The Ti^{IV}, however, is very similar radius to Nb^{V}, and the stabilization of SOMS by increasing Ti^{IV} may be attributed to increased H-bonding within the pores.

The SOMS materials have provided a unique opportunity to investigate form−function properties of a class of ion exchanger materials. Our investigations have shown that varying the Nb^{V}/M^{IV} framework composition directly varies the proton population within the channels which in turns controls properties such as ion exchange behavior and thermal stability. Drawing from

(38) Anderson, M. T.; Vaughey, J. T.; Poeppelmeier, K. R. *Chem. Mater.* **1993**, *5*, 151.
(39) Behrens, E. A.; Sylvester, P.; Clearfield, A. *Environ. Sci. Technol.* **1998**, *32*, 101.
(40) Harmon, H.; Schlahta, S.; Kent, T.; Wester, D.; Rueter, K.; Fink, S. Savannah River Site Salt Processing Project research Development Plan, PNNL-13253, Richland, WA, Tanks Focus Area, 2000.
(41) Tanks Focus Area Web Site, http://www.pnl.gov/tfa.

this knowledge we may further modify this class of materials to develop or enhance other unique properties of the SOMS materials. Furthermore, a full understanding of the SOMS class of materials may also lead to the rational design of other classes of materials that are tailored for a specific property such as ion exchange.

Acknowledgment. Sandia (T.M.N. and M.N.) is a multiprogram laboratory operated by Sandia Corporation, a Lockheed Martin Company, for the United States Department of Energy under contract DE-AC04-94AL85000. M.N. and T.M.N. thank the DOE Environmental Management Science Program (EMSP) for funding for this work. The NMR work (R.S.M.) was performed under the auspices of the U.S. Department of Energy by University of California Lawrence Livermore National Laboratory under contract No. W-7405-Eng-48. The authors thank Regina Simpson and David Tallant of Sandia National Laboratories for the Raman Spectroscopy data collection and interpretation, Yong Jae Lee for assistance with the in situ variable temperature X-ray diffraction experiments at BNL, NSLS, and Francois Bonhomme for help with Rietveld refinement.

JA017081Z